PROBA-V Collection 2
Algorithm change document

v1.00, March 2023

VITO NV
Boeretang 200 - 2400 MOL - BELGIE
Tel. + 32 14 33 55 11 - Fax + 32 14 33 55 99
vito@vito.be - www.vito.be

BTW BE-0244.195.916 RPR (Turnhout)
Bank 375-1117354-90 ING
BE34 3751 1173 5490 - BBRUBEBB

TABLE OF CONTENTS

LIST OF FIGURES

LIST OF TABLES

LIST OF ACRONYMS

ACIX	Atmospheric correction intercomparison excercise
AOT	Aerosol Optical Thickness
ARD	Analysis ready data
C1	Collection 1
C2	Collection 2
CEOS	Committee on Earth Observation Satellites
COG	Cloud Optimized Geotiff
DC	Dark Current
DCC	Deep Convective Clouds
DN	Digital Number
ESA	European Space Agency
HDF	Hierarchical Data Format
HF	High frequency
ICP	Instrument Calibration Parameters
LF	Low frequency
MERRA	Modern-Era Retrospective analysis for Research and Applications
MLP	Multi-layer perceptron
NDSI	Normalized Difference Snow Index
NDVI	Normalized Difference Vegetation Index
NIR	Near-infrared
NRT	Near-real time
OSCAR	Optical Sensor CAlibrationwith simulated Radiances
OSCARS	OpenSearch CAtalogue for Remote Sensing
PROBA	PRoject for OnBoard Autonomy
S/C	Spacecraft
SMAC	Simplified Model for Atmospheric Correction
SPOT	Satellite Pour l'Observation de la Terre
SWIR	Shortwave infrared
TOA	Top-of-Atmosphere
TOC	Top-of-Canopy
VGT	VEGETATION instrument on-board SPOT satellite
VIS	Visual bands
VNIR	Visual and near-infrared

CHAPTER 1 INTRODUCTION

1.1. INTRODUCTION

In 2020-2022, the second reprocessing campaign of the entire PROBA-V archive was performed, aiming at improving the time series and harmonizing its content. The resulting archive is PROBA-V Collection 2 (C2), covering the period 16 October 2013 – 30 June 2020.

The main modifications in the PROBA-V processing chain from C1 to C2 are:

- updates on the radiometric instrument calibration parameter (ICP) files;
- an improved cloud detection algorithm and improved cloud shadow detections;
- an improved atmospheric correction scheme;
- harmonisation of the compositing among the resolutions;
- a minor change in geometric processing.

In addition, the product format was updated to Cloud Optimized Geotiff (COG), in addition to the regular HDF5 format. Data are also available through a new catalogue (OpenSearch CAtalogue for Remote Sensing, OSCARS). Finally, PROBA-V Top-of-Canopy (TOC) reflectance data C2 data will be CEOS-ARD-compliant.

For a detailed description of the PROBA-V C2 dataset and its quality, see the PV C2 Product User Manual and the PV C2 Validation report.

1.2. SCOPE AND OBJECTIVES

This report provides a summary of the algorithm changes in C2 and describes expected impacts on the data. The following paragraphs describe the different changes that were implemented in the PROBA-V reprocessing campaign. The new reprocessed data will be referred to as 'Collection 2' (C2), and identified as .v2xx in the file naming. The old collection will be referred to as 'Collection 1' (C1), identified as .v1xx in the file naming.

1.3. RELATED SOURCES OF DOCUMENTATION

Table 1: Reference documentation for PROBA-V collection 2

Document ID	Document and link
PV C2 Product User Manual	PROBA-V C2 Product User Manual https://proba-v.vgt.vito.be/sites/probavvgt/files/downloads/PROBA-V_C2_Products_User_Manual.pdf
PV C2 Validation report	Validation report of PROBA-V Collection 2 https://proba-v.vgt.vito.be/sites/probavvgt/files/downloads/PROBA-V_C2_Evaluation.pdf
ATBD AC	Algorithm Theoretical Basis Document of the Atmospheric Correction of PROBA-V C2 https://proba-v.vgt.vito.be/sites/probavvgt/files/downloads/PROBA-V_C2_Atmospheric_Correction_ATBD.pdf

VR AC	Validation report of the Atmospheric Correction of PROBA-V C2 https://proba-v.vgt.vito.be/sites/probavvgt/files/downloads/PROBA-V_C2_Atmospheric_Correction_Validation_Report.pdf
ATBD PC	Algorithm Theoretical Basis Document of the Pixel Classification of PROBA-V C2 https://proba-v.vgt.vito.be/sites/probavvgt/files/downloads/PROBA-V_C2_Cloud_Mask_ATBD.pdf
VR PC 1 km	Validation report of the Pixel Classification of PROBA-V C2 at 1 km https://proba-v.vgt.vito.be/sites/probavvgt/files/downloads/PROBA-V_C2_Cloud_Mask_1km_Validation_Report.pdf
VR PC 300 m	Validation report of the Pixel Classification of PROBA-V C2 at 300 m https://proba-v.vgt.vito.be/sites/probavvgt/files/downloads/PROBA-V_C2_Cloud_Mask_300m_Validation_Report.pdf
VR PC 100 m	Validation report of the Pixel Classification of PROBA-V C2 at 100 m https://proba-v.vgt.vito.be/sites/probavvgt/files/downloads/PROBA-V_C2_Cloud_Mask_100m_Validation_Report.pdf

CHAPTER 2 REPROCESSING CHANGES

2.1. UPDATES ON THE RADIOMETRIC ICP FILES

Due to the absence of on-board calibration devices, the radiometric calibration and stability monitoring of the PROBA-V instrument relies solely on vicarious calibration approaches. The Optical Sensor CAlibration with simulated Radiance (OSCAR) Calibration/Validation facility (Sterckx et al., 2014), which was developed for the PROBA-V mission, contains a range of vicarious methods such as lunar calibration, calibration over stable desert sites, deep convective clouds (DCC), and Rayleigh scattering (Sterckx et al., 2016).

Long-term vicarious calibration results showed a non-linear trend in the radiometric response, which might be linked to temperature changes (both increase and decrease of temperature) over the mission lifetime, that are camera and band dependent and not considered in the Collection 0 radiometric Instrument Calibration Parameter (ICP) files. For some bands even an increasing trend is observed. The proposed solution on how to correct it in the C2 reprocessing is to apply a second-degree polynomial model.

For the reprocessing of PROBA-V C2, some changes were made to the radiometric ICP files. These include the following improvements:

- The dependence of ICP on date since launch is modeled by a 2nd degree polynomial for trending of the absolute calibration coefficients for the different strips/bands. The model also corrects for the increasing trend observed in some bands. A correction of inter-camera bias in the Blue and SWIR band is applied.
- Improvements are made in the low and high frequency multi-angular coefficients (i.e. equalization) for the SWIR strips of all cameras based on yaw maneuver results.

The aim of the adjusted absolute calibration is to better characterize the conversion of digital counts measured by the instruments into Top-of-Atmosphere (TOA) reflectance or radiance. The improved equalization coefficients on the other hand correct for inter-pixel variations over the field-of-view.

Note that the calculation of the Dark Current (DC) remains unchanged. All DC values are taken directly from the Image Quality Center database; no reprocessing was needed.

In the calculation of the TOA radiance L_{TOA} from the observed digital number (DN), both the absolute and equalization coefficients need to be taken into account simultaneously:

$$\boldsymbol{L_{TOA,i,k}} \sim \frac{\boldsymbol{DN_{i,k}} - \boldsymbol{DC_{i,k}}}{\boldsymbol{A_k}.\boldsymbol{g_{i,k}}}$$

with $\boldsymbol{A_k}$ the absolute calibration which is a function of time and spectral band

$\boldsymbol{g_{i,k}}$ the pixel relative sensitivity or equalization coefficient which varies over the field of view, time and spectral band

$\boldsymbol{DN_{i,k}}$ raw digital output number

$\boldsymbol{DC_{i,k}}$ pixel dark current

$\boldsymbol{i}$ across track pixel

$\boldsymbol{k}$ spectral band

New ICP files are created for every month, for the total reprocessing period (October 2013 – June 2020). Some more detail of these changes are given in the paragraphs below.

2.1.1. UPDATE OF THE ABSOLUTE CALIBRATION COEFFICIENTS

In C1, a step-wise linear degradation model was applied to some bands and cameras to characterize the change in radiometric responsivity. For C2, the change in radiometric responsivity is modelled for all bands and strips using a 2nd order degradation model. The results were derived based on observations over Lybia-4 and verified on the basis of Niger-2 and Lunar calibration results for the CENTER camera. A good consistency was obtained between the two sites with differences well below 1%.

The long-term analysis of all calibration results over the Libya-4 calibration site for the different cameras indicated a time-dependent inter-camera bias for the LEFT blue and SWIR right bands compared to the other cameras. For LEFT BLUE, a bias correction of 1% increase in TOA reflectance was applied. Also for SWIR RIGHT, a strip-depended bias correction was applied.

Figure 1 shows the temporal evolution of the change of the absolute calibration of Proba-V C2 with respect to C1 ($A_{k,C1}$-$A_{k,C2}$). Positive values indicate that the absolute calibration coefficient of C1 ($A_{k,C1}$) was larger compared to C2 ($A_{k,C2}$), resulting in higher TOA radiances in C2, and negative values indicate the opposite. The average difference in absolute calibration between C1 and C2 is shown in Table 1. Figure 1 and Table 1 thus show the combined effect of the degradation model and this bias correction.

Table 2: Average difference of absolute calibration ($A_{k,C1}$-$A_{k,C2}$) over the Proba-V lifetime.

	BLUE	RED	NIR	SWIR1	SWIR2	SWIR3
LEFT	1.77%	-0.56%	0.13%	-1.29%	-0.90%	-1.12%
CENTER	0.85%	-0.51%	0.27%	-0.39%	-0.18%	0.23%
RIGHT	0.14%	-0.85%	-0.57%	-0.38%	-0.60%	1.51%

In C1, minor non-linearity corrections for VNIR were applied for the C1 reprocessing (from the start of the mission until November 2016), but not for the C1 operational processing (from November 2016 till end of mission). This is solved in C2.

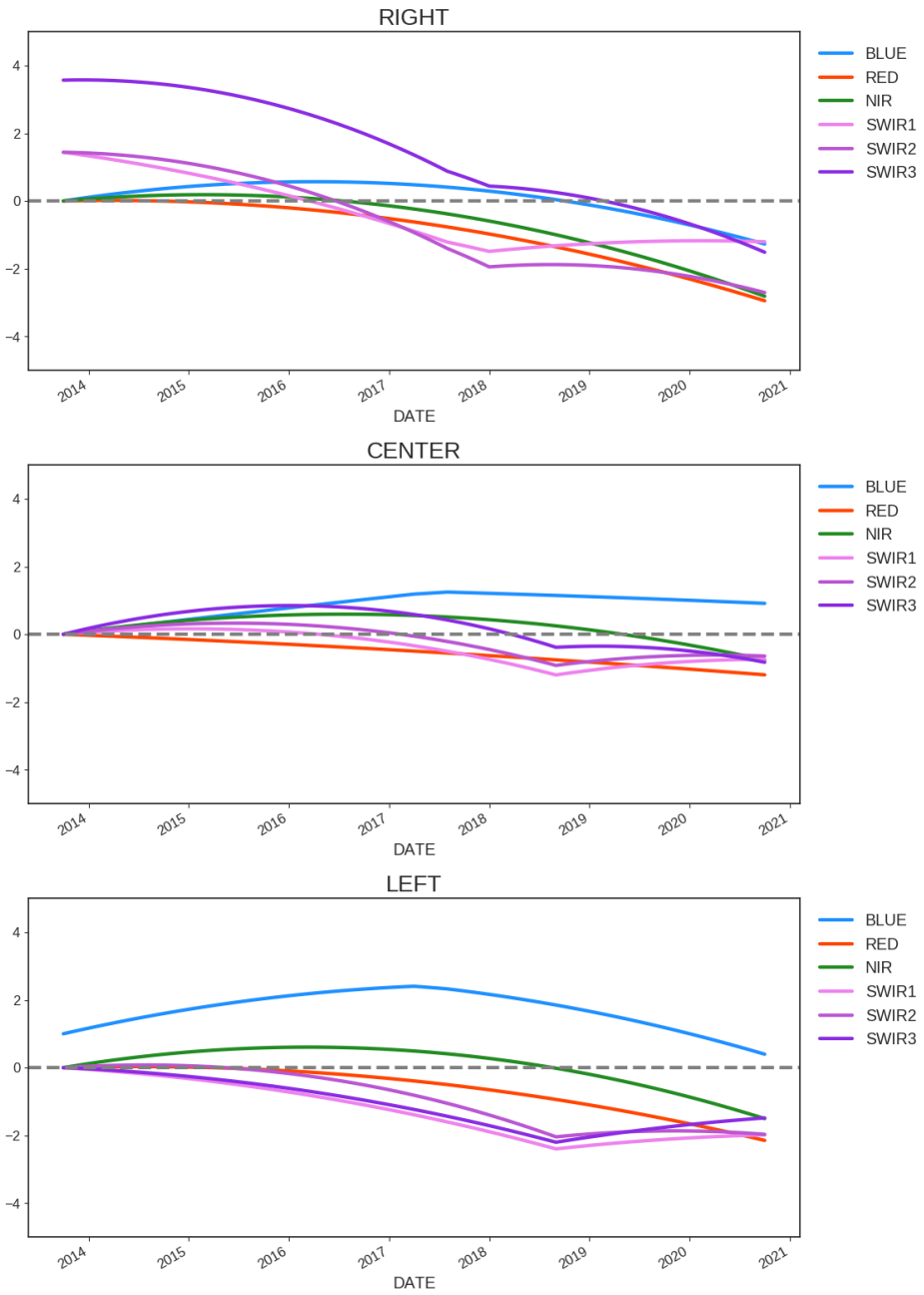

Figure 1: Percentage change of the absolute calibration coefficients of Proba-V C2 w.r.t. Proba-V C1 ($A_{k,C1}$-$A_{k,C2}$) per camera and per SWIR strip. Higher absolute calibration coefficients result in lower TOA radiances.

2.1.2. IMPROVEMENT MULTI-ANGULAR CALIBRATION SWIR STRIPS OF ALL CAMERAS

In order to better characterize and to correct for non-uniformities within and between detectors, several 90° yaw maneuvers have been performed with PROBA-V over the Niger-1 desert site. With this 90° yaw configuration, the detector array runs parallel to the direction of the motion and an area on the ground is subsequently viewed by the different pixels of the strip (Sterckx et al., 2016) (Figure 2). Improved low and high frequency (LF and HF) multi-angular calibration coefficients have been derived for each SWIR strip of each camera, leading to changes to the equalization coefficients of the different SWIR strips (Figure 3).

In Collection 1, the following updates to the equalization coefficients were made:

- CENTER camera: LF corrections based on yaw maneuver from 2016 used from 2013 until the end of the mission
- LEFT/RIGHT camera: LF+HF corrections based on yaw maneuver applied only from July 2019 until the end of the mission based on yaw maneuver data analysis from 2017/2018

In Collection 2, the following updated to the equalization coefficients are made:

- CENTER camera:
  - LF corrections from Oct 2013 based on yaw maneuver from 2016 until Dec 2015
  - LF+HF corrections based on yaw maneuver from 2016 from Jan 2016 until the end of the mission
- LEFT/RIGHT camera:
  - LF corrections from Oct 2013 until Dec 2016
  - LF+HF from Jan 2017 until the end of the mission

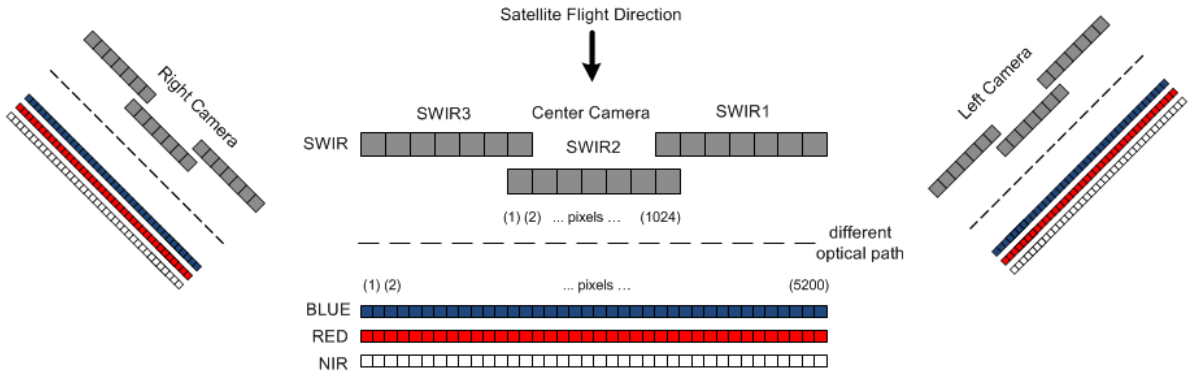

Figure 2: Definition of the cameras and the SWIR strips

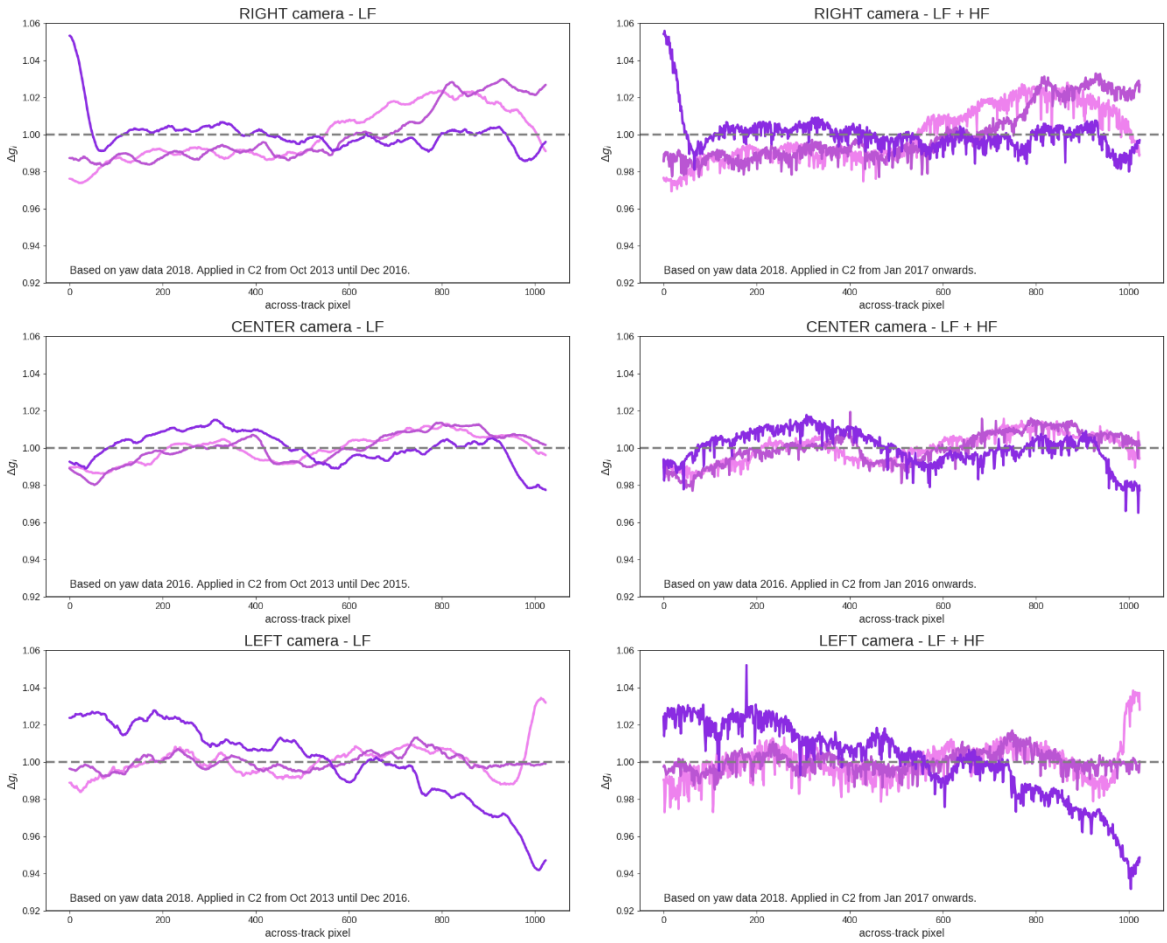

Figure 3 Changes to the equalization over the field of view (Δg_i) for the three SWIR strips per camera. Values lower than 1 result in an increase in the TOA radiance, and vice versa.

2.2. IMPROVED CLOUD DETECTION ALGORITHM

For the Collection 2 cloud and snow/ice detection, a Multi-Layer Perceptron (MLP) neural network approach developed by University of Valencia was implemented at VITO. Main rationale for implementing this algorithm was to remove the auxiliary background data dependency that was present for C1. In addition, the MLP algorithm shows significant improvements in both cloud and snow/ice detection. A schematic of the MLP algorithm is shown in Figure 4.

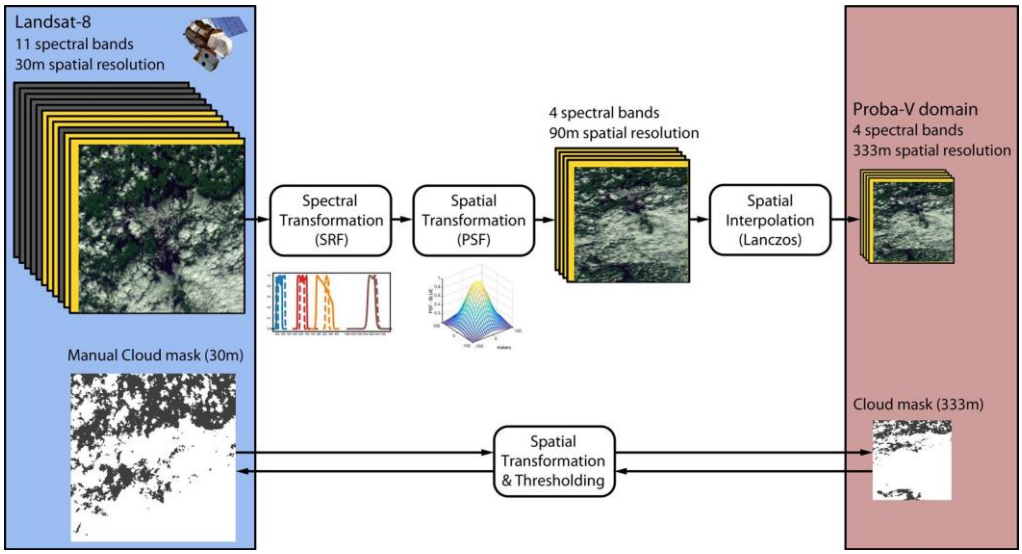

Figure 4: Schematic of the Collection 2 cloud detection algorithm

The cloud masking relies on the combination of 10 physically-based spectral features (brightness and whiteness) and spatial features derived from Level-2A TOA reflectances (Table 3). The spatial features comprise the mean and standard deviation at two different scales in 3 × 3 and 5 × 5 windows. The supervised classifiers thus use a high number of input features, though the number was limited to the 40 most relevant ones (Gómez-Chova et al., 2017). The method was further refined using upscaled Landsat images (Mateo-Garcia et al., 2021). More details can be found in the ATBD of the Pixel Classification.

Table 3: Cloud features extracted from PROBA-V L2A TOA reflectances. Adopted from Gómez-Chova et al. (2017)

Cloud Feature	Feature
Brightness	x_{Br}
Brightness VIS	$x_{Br,VIS}$
Brightness NIR	$x_{Br,NIR}$
Whiteness	x_{Wh}
Whiteness VIS	$x_{Wh,VIS}$
Whiteness NIR	$X_{Wh,NIR}$
Snow NDSI NIR	$X_{(BLUE-NIR)/(BLUE+NIR)}$
Snow NDSI SWIR	$X_{(BLUE-SWIR)/(BLUE+SWIR)}$
RED-SWIR ratio	$X_{RED/SWIR}$
NDVI	$X_{(NIR-RED)/(NIR+RED)}$

The MLP algorithm simultaneously detects clouds, and snow/ice covered surfaces. The algorithm was trained and is applied independently on the different PROBA-V resolutions. The results were validated using an extensive and globally distributed ground-truth dataset based on manual labelling.

The new cloud detection method was validated for each resolution separately and the results of this validation are summarized in the VR of Pixel Classification for the 1 km products, in the VR of Pixel Classification for the 300 m products and in the VR of Pixel Classification for the 100 m products. The validation is performed with a manually selected pixel collection and by comparison of the different cloud flags in randomly selected PROBA-V images.

Overall, the C2 cloud detection significantly improved relative to the C1 cloud detection. The main improvements are:

- Cloud under-detection (omission errors) during northern hemisphere winter months are significantly reduced.
- Generic cloud over-detection (commission errors) have been reduced.
- Better separation between clouds and snow/ice.

Due to the intrinsic cloud detection difficulties related to the limited spectral information available from the four PROBA-V spectral bands, in the following situations the MLP performance is still limited:

- Over salt lakes and urban areas (both highly reflective), some cloud over-detection was observed.
- Thin semi-transparent clouds are only detected for ~50%, with the detection being further limited with decreasing cloud (optical) thickness.
- Pixels that are fractionally covered with snow and/or contain melting ice are not detected.

An example of the cloud and snow/ice detection improvements achieved in Collection 2 is shown in Figure 5. The top panels show S1 TOC 300 m false-colour composites for Collection 2 (C2, left) and Collection 1 (C1, right). The lower panels show the obtained cloud and snow/ice detection for both Collections. The improvements for Collection 2 are evident and show a much better distinction between clouds and snow/ice, while in C1 a considerable amount of snow/ice-covered surface was incorrectly determined as cloud.

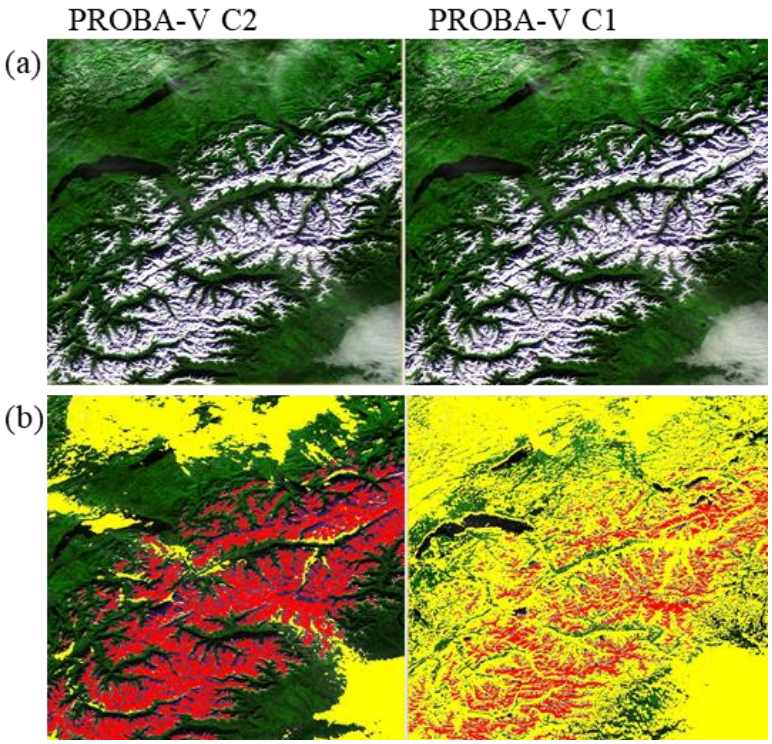

Figure 5: Visual comparison of PROBA-V L3 S1 TOC 300 m C2 (left) and C1 (right) for 21 December 2014: (a) false-colour composite (RED-NIR-BLUE), (b) overlay with cloud (yellow) and snow/ice identification (red) (Toté et al., 2021)

The cloud shadow detection is done in a different step. The method used for the previous collections was updated in Collection 2 to remove the 1 pixel gap between cloud and cloud shadow that was always present.

2.3. IMPROVED ATMOSPHERIC CORRECTION

The Collection 2 atmospheric correction has the following modifications compared to Collection 1 (see also the Algorithm Theoretical Basis Document of the Atmospheric Correction):

- The complementary combination of an image-based Aerosol Optical Thickness (AOT) retrieval and a static latitudinal AOT function in Collection 1 was replaced with dynamic AOT input from the Modern-Era Retrospective analysis for Research and Applications, version 2 (MERRA-2) (Gelaro et al., 2017).
- An exhaustive validation was performed on the resulting top-of-canopy (TOC) reflectances.

As in C1, the atmospheric correction is also based on the Simplified Model for Atmospheric Correction (SMAC, Rahman and Dedieu, 1994). In C2, an external dataset is used for the inputs of the inputs of the atmospheric correction, namely MERRA-2 (Gelaro et al., 2017). Various aerosol models were tested as input in the validation.

The obtained TOC reflectances were validated using the approach applied in the Atmospheric Correction Intercomparison eXercise (ACIX, Doxani et al., 2018). The C2 modifications lead to an improved characterisation of TOC reflectances, as well as a removal of AOT retrieval artefacts that were mainly visible in the Collection 1 BLUE and RED TOC reflectances (see the Validation report of the Atmospheric Correction of PROBA-V C2). Figure 6 shows the intercomparison of SMAC-derived TOC reflectances with those obtained from ground-based AERONET aerosol optical properties, PROBA-V TOA reflectances, and viewing and illumination angles as input. There was not a clear distinction between using the continental AOT model or using various AOT models, therefore the continental AOT model was chosen.

The validation also showed that artefacts due to the image based Aerosol Optical Thickness (AOT) retrieval are removed.

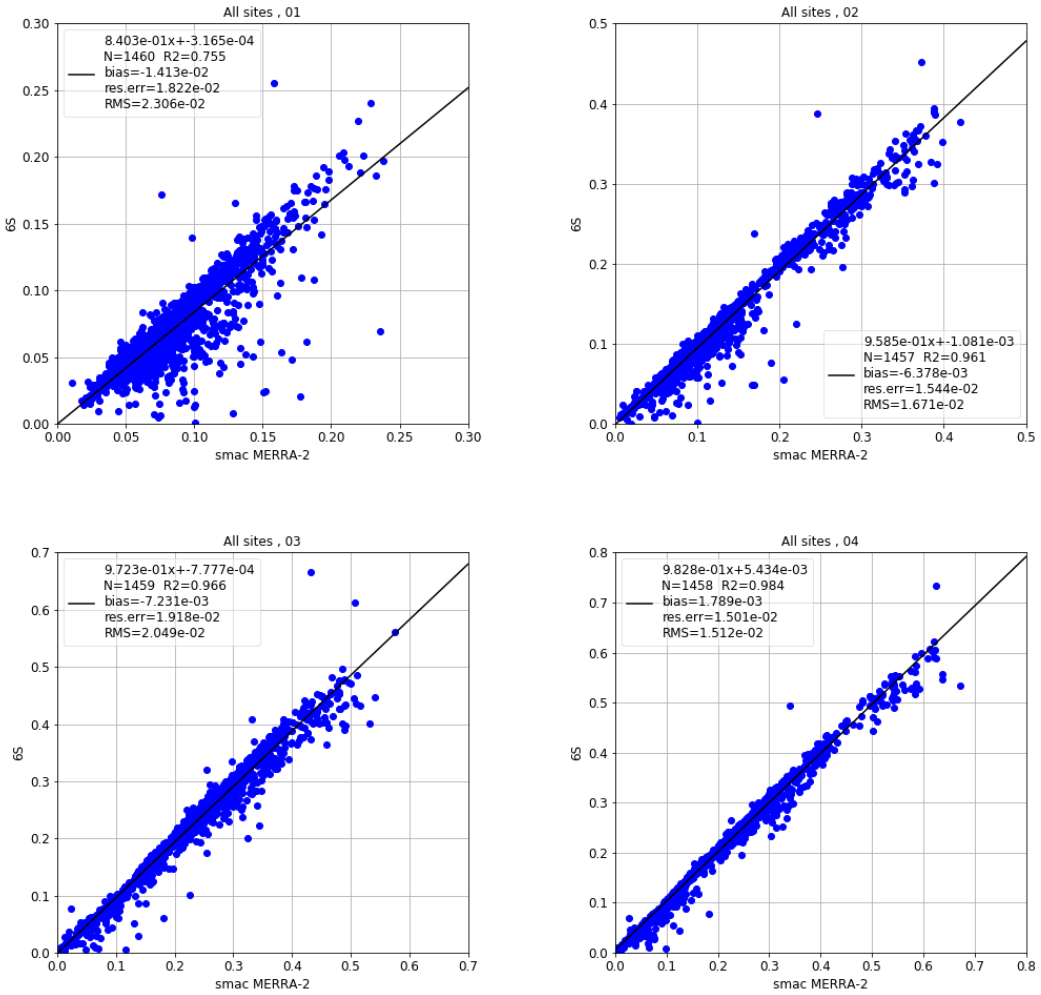

Figure 6: Comparison of TOC reflectances for the 4 PROBA-V spectral bands obtained using SMAC on MERRA-2 AOT (X-axis) and TOC reflectances processed with 6S-AERONET input (Y-axis) over 48 AERONET stations for 2018

2.4. UPDATE AND HARMONIZATION OF THE COMPOSITING METHOD

The compositing method is harmonized between the different resolutions in C2. Previously, for 100 m and 300 m the radiometric quality of all 4 bands were checked prior to compositing. Since the SWIR band has quite a number of defect detectors, this resulted in composites with a striping effect. For the 1 km, the SWIR radiometric quality was not checked in the compositing process. This method is now applied to all resolutions.

In addition, in the previous collections, if all bands had a radiometric quality 'bad', then the pixels were set to 'undefined' in the compositing step. This rule is omitted in the Proba-V C2 processing. If this situation occurs, the pixels will now have radiometric quality 'bad'.

2.5. CHANGE IN GEOMETRIC PROCESSING

In Collection 1, following geometric quality checks were performed:

(1) First, it was checked whether the individual spacecraft (S/C) roll, pitch or yaw angle (derived from the provided S/C quaternion value) exceeded a configurable threshold value (i.e. 0.015°). If at least one of the angle values exceeded the threshold value, the quaternion was considered as an outlier and the corresponding acquisition line was flagged as “bad”.
(2) If check (1) passed, the on-ground geometric distortion was calculated based on the provided S/C roll, pitch and yaw angle and checked against a configurable threshold value (i.e. 150 meter). In case the calculated error exceeded the threshold value, the quaternion was considered as an outlier and the corresponding acquisition line was flagged as “bad”.

Spikes in the individual S/C roll, pitch or yaw angle leaded to check (1) being fulfilled, which caused a lot of acquisition lines to be flagged as “bad”, although the calculated on-ground geometric distortion (check (2)) could still be below the threshold. As check (1) was considered too strict, it was decided to remove it from the Collection 1 NRT processing from 06/11/2019 onwards. In Collection 2, check (1) was removed for the entire series (i.e. only check (2) is applied).

Since check (1) was removed in the processing of Collection 2, it can be expected that there are considerably less lines in Collection 2 that are marked as “bad” compared to Collection 1. This should have a positive effect on product completeness.

Another consequence of this change is that segments for which the first or last scanlines were flagged as “bad” in C1 but not in C2 are impacted in the projection step, i.e. from sensor geometry to projected grid: the projection algorithm makes use of the first and last scanlines to define an intermediate Mercator projection in order to establish the relation between the pixels in sensor geometry and pixels in the projection grid. In these cases, the projection algorithm will use a different set of scanlines in C2 compared to C1, which implies a slightly change in the geolocation. This change can be neglected and it is not impacting the overall geolocation accuracy.

2.6. UPDATE OF THE PRODUCT FORMAT AND METADATA

In Collection 1, PROBA-V product files were available as HDF5 and GeoTiff files. In Collection 2, the HDF5 format is still available, but the alternative GeoTiff format has been replaced with the Cloud Optimized GeoTiff (COG) format. A COG is a GeoTIFF file with an internal organization that enables more efficient workflows in cloud environments. It does this by leveraging the ability issuing client HTTP GET range requests to query just the parts of a file that are needed. COG is backwards compatible with C1 GeoTIFF format. More information on the COG file format can be found at https://www.cogeo.org/.

The PROBA-V C2 metadata also received an update to allow for minimum compliancy with the CEOS Analysis Ready Data for Land (CEOS-ARD). This allows for immediate analysis and interoperability both through time and with other datasets.

REFERENCES

Doxani, G., Vermote, E., Roger, J.C., Gascon, F., Adriaensen, S., Frantz, D., Hagolle, O., Hollstein, A., Kirches, G., Li, F., Louis, J., Mangin, A., Pahlevan, N., Pflug, B., Vanhellemont, Q., 2018. Atmospheric correction inter-comparison exercise. Remote Sens. 10, 1–18. https://doi.org/10.3390/rs10020352

Gelaro, R., McCarty, W., Suárez, M.J., Todling, R., Molod, A., Takacs, L., Randles, C.A., Darmenov, A., Bosilovich, M.G., Reichle, R., Wargan, K., Coy, L., Cullather, R., Draper, C., Akella, S., Buchard, V., Conaty, A., da Silva, A.M., Gu, W., Kim, G.K., Koster, R., Lucchesi, R., Merkova, D., Nielsen, J.E., Partyka, G., Pawson, S., Putman, W., Rienecker, M., Schubert, S.D., Sienkiewicz, M., Zhao, B., 2017. The modern-era retrospective analysis for research and applications, version 2 (MERRA-2). J. Clim. 30, 5419–5454. https://doi.org/10.1175/JCLI-D-16-0758.1

Gómez-Chova, L., Mateo-García, G., Muñoz-Marí, J., Camps-Valls, G., 2017. Cloud detection machine learning algorithms for PROBA-V, in: 2017 IEEE International Geoscience and Remote Sensing Symposium (IGARSS). IEEE, pp. 2251–2254. https://doi.org/10.1109/IGARSS.2017.8127437

Mateo-Garcia, G., Laparra, V., Lopez-Puigdollers, D., Gomez-Chova, L., 2021. Cross-Sensor Adversarial Domain Adaptation of Landsat-8 and Proba-V Images for Cloud Detection. IEEE J. Sel. Top. Appl. Earth Obs. Remote Sens. 14, 747–761. https://doi.org/10.1109/JSTARS.2020.3031741

Rahman, H., Dedieu, G., 1994. SMAC: a simplified method for the atmospheric correction of satellite measurements in the solar spectrum. Int. J. Remote Sens. 15, 123–143. https://doi.org/http://dx.doi.org/10.1080/01431169408954055

Sterckx, S., Adriaensen, S., Dierckx, W., Bouvet, M., 2016. In-Orbit Radiometric Calibration and Stability Monitoring of the PROBA-V Instrument. Remote Sens. 8, 546. https://doi.org/10.3390/rs8070546

Sterckx, S., Benhadj, I., Duhoux, G., Livens, S., Dierckx, W., Goor, E., Adriaensen, S., Heyns, W., Van Hoof, K., Strackx, G., Nackaerts, K., Reusen, I., Van Achteren, T., Dries, J., Van Roey, T., Mellab, K., Duca, R., Zender, J., 2014. The PROBA-V mission: image processing and calibration. Int. J. Remote Sens. 35, 2565–2588. https://doi.org/10.1080/01431161.2014.883094

Toté, C., Swinnen, E., Sterckx, S., Benhadj, I., Dierckx, W., Gomez-Chova, L., Ramon, D., Stelzer, K., Van den Heuvel, L., Clarijs, D., Niro, F., 2021. The Reprocessed Proba-V Collection 2: Product Validation, in: 2021 IEEE International Geoscience and Remote Sensing Symposium IGARSS. IEEE, pp. 8084–8086. https://doi.org/10.1109/IGARSS47720.2021.9553376